

Experimental framework for identifying inconsistent measurements in frequency-based substructuring

Miha Kodrič^a, Gregor Čepon^{a,*}, Miha Boltežar^a

^a*University of Ljubljana, Faculty of Mechanical Engineering, Aškerčeva 6, 1000 Ljubljana, Slovenia*

Cite as:

*Miha Kodrič, Gregor Čepon, Miha Boltežar,
Experimental framework for identifying inconsistent measurements in frequency-based substructuring,
Mechanical Systems and Signal Processing, 2021,
<https://doi.org/10.1016/j.ymssp.2020.107562>*

Abstract

The dynamic properties of modern products are analysed using an experimental approach through the measurement of frequency-response functions (FRFs). For an individual measurement, the coherence offers an online check during the system acquisition. More general tools for determining the consistency of the complete measurement set are based on a comparison of the FRFs or the modal shapes with a numerical model. They are useful tools, but they rely on a comparison with a numerical model that might not reflect the behaviour of the actual system. This paper aims to develop a comprehensive experimental method to check the consistency of individual measurements based on comparisons with the complete experimental response model. The numerical model is introduced only to enable the experimental model to be expanded using the System Equivalent Model Mixing method. The entire formulation is developed in the frequency domain, so that the transition to the modal domain, which might remove the physically relevant information from the system, is not required. In the frequency domain, it is possible to assess the consistency of the FRF across the entire frequency range of interest and not only in the region of the natural frequencies. This is of great importance in the area of frequency-based substructuring, where even small inaccuracies in the substructure's FRFs (e.g.,

*Corresponding author

Email address: `gregor.cepon@fs.uni-lj.si` (Gregor Čepon)

the position of the anti-resonance) can lead to erroneous coupling results due to the inversion process. The experimental case study demonstrates the efficiency of the proposed approach. By removing the identified inconsistent measurements, it was possible to significantly increase the accuracy of the final coupling process.

Keywords: Measurement error, Data consistency, System equivalent model mixing, Dynamic substructuring, Frequency domain, Expansion process, Experimental model

1. Introduction

The analysis of structural dynamics is an essential step in the design of high-tech mechanical systems. This generally requires the creation of virtual dynamics models of the system components, which can be assembled to evaluate the dynamic properties of the complete product. Dynamic substructuring methods can be seen as a domain-independent set of tools for combining the characteristics of the structural dynamics [1]. Efficient substructuring techniques accelerate the finite-element analysis and enable the vibro-acoustic optimization of complex systems. Numerical substructuring methods have gained acceptance over the years; however, with increasing product complexity the question arises as to how we can accurately, using only numerical models, represent the actual behaviour of the individual components of the whole system.

In recent years, the structural dynamics community showed a renewed interest in structure-coupling techniques, especially in the context of experimental applications [2]. This led to an increase in the experimental modelling of relatively complex structures. Yet stand-alone experimental models¹ are strongly influenced by essentially independent and often imperfect measurements [3]. This is particularly so for the Lagrange Multiplier Frequency-Based Substructuring (LM FBS) method, which is based on response models and was formulated by de Klerk et al. [4]. The LM FBS method is normally related to the experimental approach, as it is possible to directly define the real dynamics properties based on the measured Frequency Response Functions (FRFs). The method's application to complex, real-life engineering structures is often hindered by its notorious sensitivity

¹The phrase experimental model denotes an admittance matrix that is obtained by directly measuring the FRFs on the structure [2].

to experimental errors [2]. It remains a challenge to extract a consistent dynamic model performed on a limited number of essentially non-collocated DoFs [5].

The LM FBS method often relies on the identification of an admittance (receptance) matrix. The method involves the inverse of the experimental admittance matrix, which is often poorly conditioned due to the experimental errors and thus prone to severe error amplification [6, 7]. In order to overcome this problem, several researchers developed methods to improve the consistency of the measurement with truncated singular-value decomposition techniques [8] or by using other filtration [9] and data-smoothing techniques [10, 11]. These methods improve the accuracy of the dynamic coupling, but do not provide any information about the quality of the measurements. In general, the measurement error can be classified into two categories according to its type: systematic (also called bias) and random. The systematic error is introduced by inaccuracies inherent to the system that can involve either the observation or the measurement process. The impact of such systematic errors on the coupling is analysed in [12, 13]. The second type of measurement error is random in nature and is referred to as the measurement uncertainty. Random errors can be evaluated and quantified with statistical tools [14, 15].

To evaluate the quality of repeated individual measurements, a coherence criterion is a valid approach and offers an online check during system acquisition. Using coherence it is possible to identify the measurement errors that are random in nature [16]. More general tools to determine the consistency of the entire measurement data set rely on a comparison of the FRFs or mode shapes. Using the FRAC [17], MAC [18], CoMAC [19], etc. criteria, gives some insight into identifying poorly correlated DoFs. They are useful tools, but they are not able to identify the relationship between the measurements inside the experimental data set. The relationships between the measurements in the experimental data set, therefore, relate to the criterion that would enable a comparison of the individual measurement with respect to other measurements in the experimental response model. These tools only allow a comparison with other data sets, usually obtained by a numerical model that might not reflect the behaviour of the actual system. Moreover, by comparing the modal shapes, only the inconsistencies in a narrow frequency range around the natural frequencies can be observed. Recently, a new, general approach called the Data Consistency Assessment Function (DCAF) [20] was proposed that is able to evaluate the consistency of a set of measurements. The basic approach is to remove one particular measurement from the complete set of data and then recreate that measurement

using the expansion technique from the remaining data set. The method is formulated in the modal domain using the SEREP expansion process. The value of the correlation coefficient is calculated based on the matching of mode shapes of the reconstructed and the original measurements using the MAC criterion.

This paper presents a new approach to the identification of inconsistent measurements in the process of dynamic substructuring. The basic idea is similar to the DCAF method of removing a measurement from the entire data set and then reconstructing it from the remaining measurement set. Here, however, the entire formulation is developed within the frequency domain. The expansion process is based on the System Equivalent Model Mixing (SEMM) method that was presented by Klaassen et al. [5]. Since the method is developed in the frequency domain, the transition to the modal domain, which can remove the physically relevant information about the real system, is not required. In the frequency domain it is possible to assess the consistency of the FRFs in the entire frequency range of interest and not only in the region of the natural frequencies. This can be done with correlation criteria that compare two different FRFs for the same input-output position, which is frequency dependent. This is particularly important in the field of frequency-based substructuring, where even small inaccuracies in FRFs (e.g., position of the anti-resonances) can lead, due to the inversion process, to erroneous coupling results. To present the capability of the introduced method, an experimental coupling of two simple beam-like structures is presented. The proposed method demonstrates the possibility of identifying small inconsistencies in the measured FRFs. Finally, we show that by removing the inconsistent FRFs from the experimental substructure model, it is possible to significantly improve the efficiency and accuracy of the coupling process.

The paper is organized as follows. The following section briefly summarizes the theory of the LM FBS and the SEMM methods. Next, the identification algorithm of an inconsistent measurement is presented in Section 3. In Section 4 an experimental validation of the proposed algorithm is performed on a laboratory, beam-like structure. Finally, the conclusions are drawn in Section 5.

2. Theoretical background

2.1. LM FBS method

The dynamic properties of substructures are often given by FRFs calculated from the responses and excitation measurements at different sub-

structure locations. The LM FBS method [4] enables the dynamic coupling of admittance matrices in which the FRFs of individual subsystems are collected. The equation of motion for a discrete dynamic subsystem s in the frequency domain is:

$$\mathbf{u}^s(\omega) = \mathbf{Y}^s(\omega) (\mathbf{f}^s(\omega) + \mathbf{g}^s(\omega)). \quad (1)$$

The vector of DoFs $\mathbf{u}^s(\omega)$ represents the responses to the external force vector $\mathbf{f}^s(\omega)$ and $\mathbf{g}^s(\omega)$ is the vector of connecting forces with the other substructures to ensure equilibrium conditions. The admittance matrix of the substructure is denoted with $\mathbf{Y}^s(\omega)$. To consider all n subsystems it is necessary to assemble their admittance matrices into a block-diagonal form:²

$$\mathbf{u} = \mathbf{Y} (\mathbf{f} + \mathbf{g}), \text{ where: } \mathbf{Y} = \begin{bmatrix} \mathbf{Y}^1 & & \\ & \ddots & \\ & & \mathbf{Y}^n \end{bmatrix}, \mathbf{u} = \begin{bmatrix} \mathbf{u}^1 \\ \vdots \\ \mathbf{u}^n \end{bmatrix}, \mathbf{f} = \begin{bmatrix} \mathbf{f}^1 \\ \vdots \\ \mathbf{f}^n \end{bmatrix}, \mathbf{g} = \begin{bmatrix} \mathbf{g}^1 \\ \vdots \\ \mathbf{g}^n \end{bmatrix}. \quad (2)$$

In the dynamic coupling process, the connections between the substructures must be defined by the compatibility and equilibrium conditions. The inclusion of both conditions is achieved with the signed Boolean matrix \mathbf{B} . The compatibility conditions are written using Eq. (3), which means that the coupled structures have the same displacements or rotations at the interface. It is necessary to provide such a space of DoFs that at the interfaces, these nodes coincide. The equilibrium conditions (Eq. (4)) are introduced by choosing the interface forces using a set of unknown Lagrange multiplier vectors $\boldsymbol{\lambda}$.

$$\mathbf{B} \mathbf{u} = \mathbf{0} \quad (3)$$

$$\mathbf{g} = -\mathbf{B}^T \boldsymbol{\lambda} \quad (4)$$

By combining the compatibility condition (Eq. (3)) and the equation of motion of the uncoupled system (Eq. (2)) and taking into account the equilibrium condition (Eq. (4)), we can determine the interface forces in the Lagrange multiplier vector:

$$\mathbf{B} \mathbf{u} = \mathbf{B} \mathbf{Y} (\mathbf{f} + \mathbf{g}) = \mathbf{B} \mathbf{Y} (\mathbf{f} - \mathbf{B}^T \boldsymbol{\lambda}) = \mathbf{0} \quad \Rightarrow \quad \boldsymbol{\lambda} = (\mathbf{B} \mathbf{Y} \mathbf{B}^T)^{-1} \mathbf{B} \mathbf{Y} \mathbf{f}. \quad (5)$$

²An explicit dependence on the frequency is omitted to improve the readability of the notation, as will be the case for the remainder of the paper.

The response of the coupled structure can be written as:

$$\mathbf{u} = \tilde{\mathbf{Y}} \mathbf{f} = \left[\mathbf{Y} - \mathbf{Y} \mathbf{B}^T (\mathbf{B} \mathbf{Y} \mathbf{B}^T)^{-1} \mathbf{B} \mathbf{Y} \right] \mathbf{f}. \quad (6)$$

The dynamic properties of the assembled system are governed by the coupled admittance matrix $\tilde{\mathbf{Y}}$:

$$\tilde{\mathbf{Y}} = \mathbf{Y} - \mathbf{Y} \mathbf{B}^T (\mathbf{B} \mathbf{Y} \mathbf{B}^T)^{-1} \mathbf{B} \mathbf{Y}. \quad (7)$$

Eq. (7) is a single-line equation of the LM FBS to couple the models and represents the basic formulation for the whole SEMM theory.

2.2. SEMM method

System Equivalent Model Mixing (SEMM) was first introduced by Klaassen et al. [5]. The method forms a hybrid structural dynamic model by mixing the numerical and experimental FRFs. The procedure applies a substructuring approach to expand the model dynamics contained in an overlay model \mathbf{Y}_{ov} onto the DoF space of a parent model \mathbf{Y}_{par} [21].

The main idea of the SEMM method is shown in Fig. 1. The method is based on the parent model (Fig. 1a), which provides the extensive DoF set. In our case the parent model was of a numerical nature, obtained by the direct frequency-response method, to avoid the effects of modal truncation, which usually occur in the modal superposition method. The dynamic properties are introduced by the overlay model (Fig. 1b), which is generally obtained by experiment. To form the final hybrid model (Fig. 1d) the dynamic properties of the parent model are eliminated with the removed model (Fig. 1c).

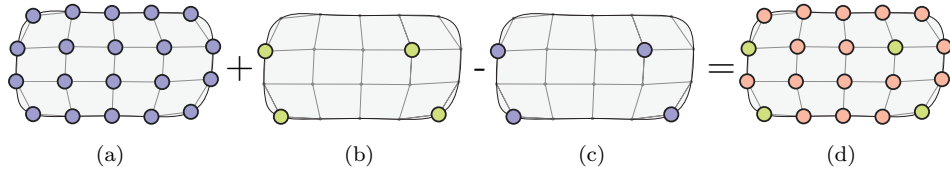


Figure 1: Equivalent models for SEMM method; a) Parent model \mathbf{Y}^{par} , b) Overlay model \mathbf{Y}^{ov} , c) Removed model \mathbf{Y}^{rem} , d) Hybrid model \mathbf{Y}^{SEMM} .

The DoF set of the parent model is contained in the internal (i) and boundary (b) DoFs. The boundary DoFs must overlap with the overlay model so that the dynamic coupling can be performed, while the internal DoFs of the parent model can be unique to its own. The equivalent models,

appearing in the SEMM method, are arranged by separating the internal and boundary DoFs in the admittance matrices:

$$\mathbf{Y}^{\text{par}} \triangleq \begin{bmatrix} \mathbf{Y}_{ii} & \mathbf{Y}_{ib} \\ \mathbf{Y}_{bi} & \mathbf{Y}_{bb} \end{bmatrix}^{\text{par}}, \quad \mathbf{Y}^{\text{ov}} \triangleq [\mathbf{Y}_{bb}]^{\text{ov}}, \quad \mathbf{Y}^{\text{rem}} \triangleq [\mathbf{Y}_{bb}]^{\text{par}}. \quad (8)$$

The LM FBS methodology is used to form a hybrid model in the SEMM method. First, the original parent model dynamic is removed with the dynamic decoupling between the parent and removed model. Next, the dynamic coupling between the parent and the overlay model, to force the overlay dynamics in the parent model, is performed, which produces a hybrid model. The hybrid model combines all three models in the admittance form. The basis equation of motion for the SEMM method can be formulated as:

$$\begin{bmatrix} \mathbf{u}^{\text{par}} \\ \mathbf{u}^{\text{rem}} \\ \mathbf{u}^{\text{ov}} \end{bmatrix} = \begin{bmatrix} \mathbf{Y}^{\text{par}} & & \\ & -\mathbf{Y}^{\text{rem}} & \\ & & \mathbf{Y}^{\text{ov}} \end{bmatrix} \begin{bmatrix} \mathbf{f}^{\text{par}} \\ \mathbf{0} \\ \mathbf{0} \end{bmatrix} - \begin{bmatrix} \mathbf{g}^{\text{par}} \\ \mathbf{g}^{\text{rem}} \\ \mathbf{g}^{\text{ov}} \end{bmatrix}. \quad (9)$$

Following the LM FBS methodology, the vector of DoFs is \mathbf{u} and represents the responses to the external force vector \mathbf{f} acting only on the parent model and \mathbf{g} is the vector of the interface forces between the equivalent models. The compatibility and equilibrium conditions between the equivalent models are defined using the following equations:

$$\mathbf{B}\mathbf{u} = 0, \quad (10)$$

$$\mathbf{g} = -\mathbf{B}^T \boldsymbol{\lambda}, \quad (11)$$

where the signed Boolean matrix is defined as:

$$\mathbf{B} \triangleq [\mathbf{B}^{\text{par}} \quad \mathbf{B}^{\text{rem}} \quad \mathbf{B}^{\text{ov}}] = \begin{bmatrix} 0 & -\mathbf{I} & \mathbf{I} & 0 \\ 0 & 0 & -\mathbf{I} & \mathbf{I} \end{bmatrix}. \quad (12)$$

Considering the compatibility (Eq. (10)) and the equilibrium (Eq. (11)) conditions in the basic equation of motion (Eq. (9)), together with the Lagrange multiplier's elimination, results in a single-line form of the SEMM method:

$$\bar{\mathbf{Y}} = \mathbf{Y} - \mathbf{Y}\mathbf{B}^T (\mathbf{B}\mathbf{Y}\mathbf{B}^T)^{-1} \mathbf{B}\mathbf{Y}, \quad \text{where: } \mathbf{Y} \triangleq \begin{bmatrix} \mathbf{Y}^{\text{par}} & & \\ & -\mathbf{Y}^{\text{rem}} & \\ & & \mathbf{Y}^{\text{ov}} \end{bmatrix}. \quad (13)$$

To retain the primary DoFs, the primary formulation must be reformulated using the localization matrix [5], which results in a single-line form of the

basic SEMM method:

$$\mathbf{Y}^{\text{SEMM}} = [\mathbf{Y}]^{\text{par}} - \begin{bmatrix} \mathbf{Y}_{\text{ib}} \\ \mathbf{Y}_{\text{bb}} \end{bmatrix}^{\text{par}} (\mathbf{Y}^{\text{rem}})^{-1} (\mathbf{Y}^{\text{rem}} - \mathbf{Y}^{\text{ov}}) (\mathbf{Y}^{\text{rem}})^{-1} [\mathbf{Y}_{\text{bi}} \quad \mathbf{Y}_{\text{bb}}]^{\text{par}}. \quad (14)$$

The basic SEMM method also has some extensions [5] that increase its robustness. The first extension removes any spurious peaks in the frequency domain with an extension of the removed interface. The secondary parent model enables us to have two parent models, where each has unique internal DoFs. The last extension includes a trust function to steer the dynamics of the hybrid model at low frequency to the parent model, due to the higher accuracy of the numerical model in this region.

The ability to remove spurious peaks, which are a consequence of the conflicting dynamics between the overlay (\mathbf{Y}^{ov}) and the removed numerical (\mathbf{Y}^{par}), is essential to improve the method's applicability [21]. If the removed interface is extended to all the internal DoFs, then the removed model has the following form:

$$\mathbf{Y}^{\text{rem}} = \begin{bmatrix} \mathbf{Y}_{\text{ii}} & \mathbf{Y}_{\text{ib}} \\ \mathbf{Y}_{\text{bi}} & \mathbf{Y}_{\text{bb}} \end{bmatrix}^{\text{par}}. \quad (15)$$

The final version of the fully extend SEMM method in a single-line notation can be written as:

$$\mathbf{Y}^{\text{SEMM}} = \mathbf{Y}^{\text{par}} - \mathbf{Y}^{\text{par}} \left([\mathbf{Y}_{\text{bi}} \quad \mathbf{Y}_{\text{bb}}]^{\text{rem}} \right)^+ (\mathbf{Y}_{\text{bb}}^{\text{rem}} - \mathbf{Y}^{\text{ov}}) \left(\begin{bmatrix} \mathbf{Y}_{\text{ib}} \\ \mathbf{Y}_{\text{bb}} \end{bmatrix}^{\text{rem}} \right)^+ \mathbf{Y}^{\text{par}}. \quad (16)$$

3. Identification of inconsistent measurements in the frequency domain

The following section presents our new method for the identification of inconsistent measurements that can influence the quality of the experimental response model and with this the accuracy of the substructuring process. The method is defined in the frequency domain and enables a consistency check of an individual measurement with regards to the entire experimental data set. To assess the quality of a single measurement, the algorithm relies on the removal of one or a set of measurements and their reconstruction based on the expansion process with the remaining measurements in the complete experimental response model. To assess the quality of the original measurement, a frequency-dependent correlation is calculated between the reconstructed and the original measurements.

The expansion process is performed using the SEMM method [5], where SEMM-expanded DoFs are used to reconstruct the measurement at the given location of an actual measurement [21]. In order to perform the SEMM expansion, a corresponding numerical model must be established that serves as the parent model. The numerical model must include at least the DoFs included in the experimental (overlay) model. Both models should have the shape of a rectangular receptance matrix. In extreme cases this can be either only one row or one column, or it may be a square matrix.

A schematic representation of the method is shown in Fig. 2, where for the sake of simplicity, four data points are considered in the experimental model and the corresponding numerical model consists of twenty data points. For a better understanding of the identification algorithm, only one row of the receptance matrix is used in the presented example. The response was measured at only one point, and the structure was excited for all four points to construct the experimental model and at all twenty points for the numerical model. The locations of measurement points must coincide with the discretization points of the numerical model. In each iteration, the removed measurement is reconstructed based on all the remaining measurements in the complete data set using the SEMM expansion. The reconstructed FRF includes the dynamics of the real structure combined with the numerical model. Let us assume that in the first step of the method the measurement at point 1 is removed so that the overlay (experimental) model contains only measurements at the locations of points 2-4 (Fig. 2). The parent (numerical) model contains all twenty DoFs and remains the same throughout the whole iteration process. With the SEMM method, the dynamic properties of the overlay (experimental) model are expanded to all the DoFs included in the parent (numerical) model. This also includes point 1, at which the measurement was removed from the overlay model. If the original measurement is consistent, it should correlate well with the reconstructed measurement based on the SEMM-expansion process, which is then repeated for all the remaining measurement points in the experimental model (points 2-4).

After the expansion process, the comparison between all the reconstructed FRFs and their original experimental counterparts is made. If the identification criterion shows a reasonable correlation between the experimental and the associated reconstructed FRF, it can be considered as a consistent measurement and remains in the experimental set. However, if the measurement proves to be inconsistent it will be completely removed from the experimental set. The comparison between the reconstructed and the original measurements can be performed using a variety of criteria, for instance, the coherence criterion compares two different FRFs for the same

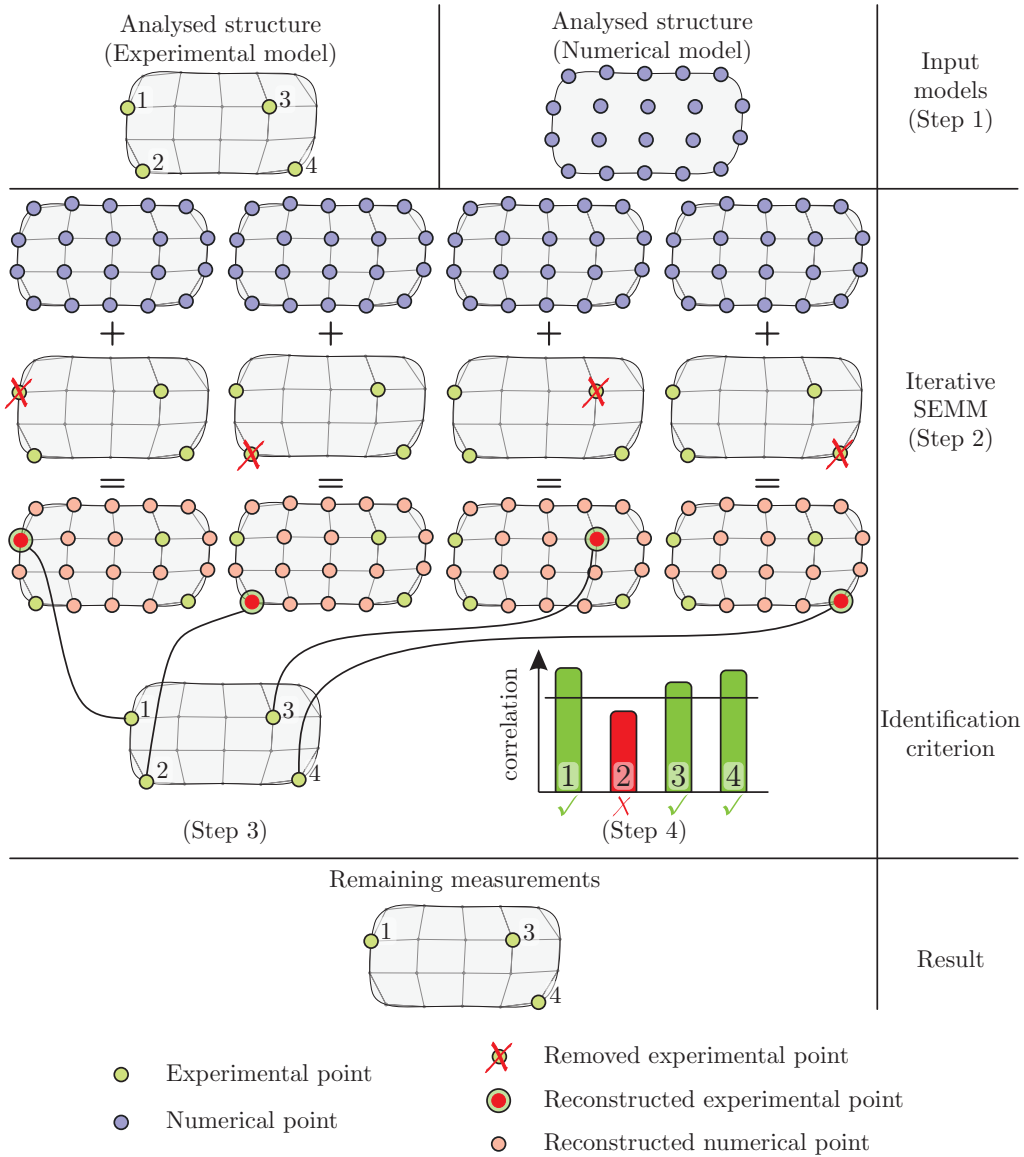


Figure 2: Proposed identification algorithm for the identification of inconsistent measurements in the frequency domain.

input-output position. The last step of the algorithm is to determine the limiting value of the identification criterion that enables the separation between the consistent and inconsistent measurements (Fig. 2). Since the basic assumption of the approach proposed in this article is that the majority of the

measurements are consistent, it is somehow clear that the limit of coherence should be set to the value where the majority of the measurement remains in the experimental response model. Taking into account this assumption, the limit is set as high as possible. It should be emphasised here that the value of the coherence is the trade-off between a high-quality measurement and the extent of the dynamics information introduced into the system by the measurement. More information regarding the identification criterion is presented in the next section.

The proposed identification algorithm for the general case of a multidimensional experimental matrix can be summarized as follows:

- (STEP 1) Define the experimental and numerical input models of the analysed structure with complementary frequency points.

$$\mathbf{Y}_{m \times n}^{\text{Exp.}} \text{ and } \mathbf{Y}_{p \times r}^{\text{Num.}} \text{ where: } m \leq p \text{ and } n \leq r$$

The parameters m and p refer to the number of rows (response locations) in the experimental or numerical model, respectively, while the parameters n and r stand for the number of columns (excitation locations) in the experimental or numerical model.

- (STEP 2) The iterative process of removing the measurement points and reconstructing them based on the SEMM-expansion process. The use of the algorithm for the multi-row or multi-column experimental receptance matrix is presented in Fig. 3.

Using Eq. (16) to combine $\mathbf{Y}_{(m-1) \times n}^{\text{Exp.}}$ or $\mathbf{Y}_{m \times (n-1)}^{\text{Exp.}}$ with $\mathbf{Y}_{p \times r}^{\text{Num.}}$

In each step of the iterative SEMM procedure, the entire row or column of the experimental receptance matrix is removed. This meets the requirement of the SEMM method that the overlay model has the shape of the rectangular matrix. Thus, multiple measurements are reconstructed simultaneously for each sub-step. It makes sense to choose such a strategy for removing the measurements, in which the reconstruction in each sub-step is based on as many remaining measurements as possible.

- (STEP 3) Calculate the correlation criterion that compares the reconstructed and measured FRFs for the same input-output position. In the general case of the multidimensional experimental receptance matrix, it is a 3D bar chart, as shown in Fig. 3.
- (STEP 4) Determination of the limit value of the identification criterion and the removal of inconsistent measurements from the experimental response model. The identified inconsistent measurements

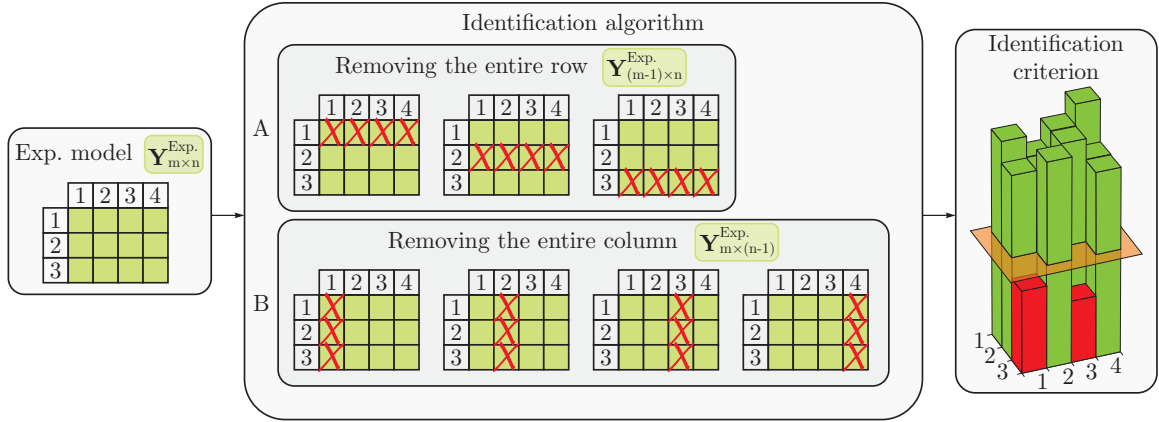


Figure 3: Strategy to remove measurements during the iterative SEMM process when analysing a multi-dimensional experimental response matrix.

can also be corrected by an expansion [21] or smoothing procedures [22].

If a specific measurement is identified as inconsistent, it can either be omitted or reconstructed using the proposed SEMM-expansion process. However, we should take into account that the reconstruction is performed using all the remaining consistent measurements, so no new information is introduced into the dynamics response model. Therefore, even if the inconsistent DoF is reconstructed and not omitted from the experimental model, this would not improve the experimental response model’s consistency. The reconstruction of the omitted DoF only makes sense when the response at the given DoF is required in the subsequent procedure.

3.1. FRF comparison techniques

To correctly compare the two FRFs, a comprehensive criterion must be introduced that considers the comparison across the entire frequency range, both in terms of amplitude and phase. For many years, it has been common practice to visually compare the FRFs, and in this way assess the level of their correlation [23]. However, in order to objectively assess the correlation, more advanced criteria were introduced. The basic method for comparing functions in the frequency domain is the frequency-response assurance criterion (FRAC) [17] and the frequency-amplitude assurance criterion (FAAC) [24] method, where the correlation between the FRFs is represented by a scalar value. More advanced criteria that enable a comparison

of the FRFs versus frequency were developed in the field of modal updating [24, 25]. In this field the so-called Local Amplitude Criterion (LAC) [24] was introduced that enables a comparison of a single measured FRF and its recreated counterparts versus frequency:

$$\text{LAC}_{ij}(f_k) = \frac{2 |Y_{ij}^{\text{Rec.*}}(f_k) Y_{ij}^{\text{Exp.}}(f_k)|}{\left(Y_{ij}^{\text{Rec.*}}(f_k) Y_{ij}^{\text{Rec.}}(f_k)\right) + \left(Y_{ij}^{\text{Exp.*}}(f_k) Y_{ij}^{\text{Exp.}}(f_k)\right)} \quad (17)$$

The variable $Y_{ij}^{\text{Rec.}}$ stands for the reconstructed measurement and $Y_{ij}^{\text{Exp.}}$ represents the real measurement. With * we denote the complex conjugate. The characteristic number for a comparison with the other measuring points is the average value of the match across all frequencies (N represents the number of considered frequency points):

$$\overline{\text{LAC}}_{ij} = \frac{1}{N} \sum_{k=1}^N \text{LAC}_{ij}(f_k). \quad (18)$$

The LAC criterion makes it possible to compare the FRFs only in terms of amplitude [26]. For this reason, Seijs et al. [27] used a coherence criterion function to evaluate the reciprocity of two FRFs. It enables a comparison in both the amplitude and phase spectra.

$$\text{coh}_{ij}(f_k) = \frac{\left(Y_{ij}^{\text{Rec.}}(f_k) + Y_{ij}^{\text{Exp.}}(f_k)\right) \left(Y_{ij}^{\text{Rec.*}}(f_k) + Y_{ij}^{\text{Exp.*}}(f_k)\right)}{2 \left(Y_{ij}^{\text{Rec.*}}(f_k) Y_{ij}^{\text{Rec.}}(f_k) + Y_{ij}^{\text{Exp.*}}(f_k) Y_{ij}^{\text{Exp.}}(f_k)\right)} \quad (19)$$

The coherence criterion allows us to estimate the correlation of two FRFs versus the frequency. To enable an overall correlation between the FRFs, an average coherence over the considered frequency range is introduced:

$$\overline{\text{coh}}_{ij} = \frac{1}{N} \sum_{k=1}^N \text{coh}_{ij}(f_k). \quad (20)$$

Both methods, the LAC and the coherence criterion, give similar results when the average value of a given criterion is compared. The difference is notable when the values of the criteria are plotted versus the frequency, as will be presented in the experimental case study.

For a credible identification, it must be assumed that in the experimental model the majority of the measurements are consistent. If this is not the case, then the reconstruction of a particular measurement is based on

erroneous FRFs and the reconstruction is meaningless. The algorithm relies on the SEMM-expansion method, hence it inherits a limitation to the linear and time-invariant systems [1]. If any of these assumptions are violated, the SEMM-expansion process would be inconsistent. Both identification criteria enable the detection of measurements containing a random error. In addition, systematic errors can be identified, such as inaccuracies in the positioning of sensors, the incorrect calibration of measurement equipment, and imperfect impact/excitation locations. The proposed algorithm can also be used to detect measurements contaminated by cable problems, clipping, misalignment of the transducer, or incorrectly labelled measurements.

4. Experimental case study

The applicability of the proposed method for the identification of inconsistent measurements is demonstrated on a simple beam structure with a rectangular cross-section. The beam A-A represents the main system assembled from two equal beams A (Fig. 4). Since the measurements were not acquired at the interface DoFs, they were reconstructed using the SEMM-expansion process. In this way, a hybrid model of beam A was constructed. The final coupling was thus performed with the two identical hybrid models of beam A using the LM FBS method. First, the experimental response model and the corresponding numerical model of beam A must be obtained (Table 1). On beam A, 26 equidistant measuring points were used (Fig. 4).

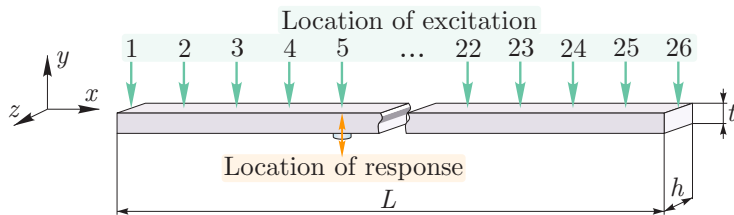


Figure 4: Schematic presentation of beam A.

Table 1: Parameters of beam A.

Parameter	Value
L	300 mm
h	40 mm
t	12 mm
E	205 GPa
ρ	7820 kg/m ³

For the numerical model, the 1D finite-element method was applied, following Timoshenko’s beam theory. The direct-force method without damping was applied to generate FRFs in the range between 0 and 7000 Hz with a frequency resolution of 1 Hz. The entire beam was discretised with 250 elements, whose 26 nodal coordinates coincided with the positions of the measurement points (Fig. 5). The FRFs in the numerical model were determined for all combinations of the excitation with the force in the y -direction

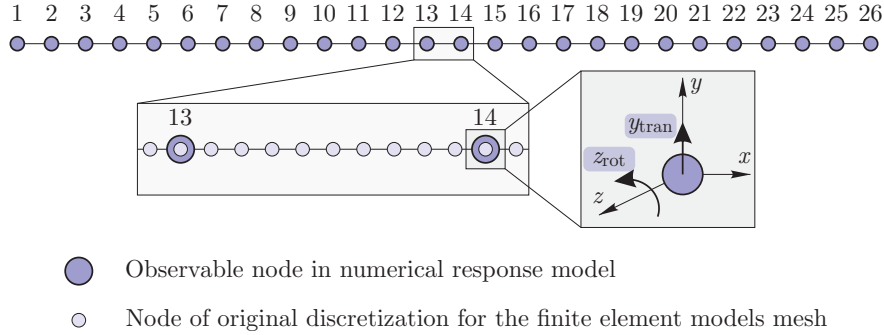


Figure 5: Numerical model of the analysed beam A.

and a torque about the z -axis. The translational response was captured in the y -direction and the rotation about the z -axis for all 26 points, considering free-free boundary conditions. The numerical model results in a square receptance matrix. For the purpose of the identification algorithm, the parent model consisted of only one row in the numerical receptance matrix, as depicted in Fig. 6.

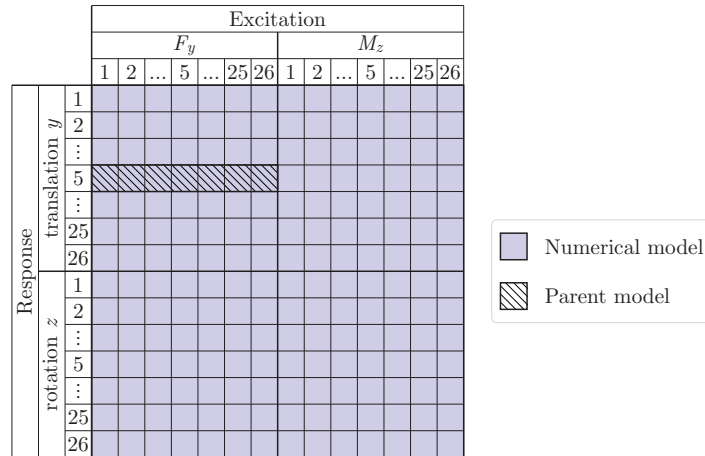


Figure 6: Schematic representation of the numerical receptance matrix.

In the experimental setup, the free-free boundary conditions were approximated by placing the beam on polyurethane foam blocks. The rowing force excitation was performed in the y -direction for all 26 points, simultaneously, the translational response was measured at point 5 in the y -direction, as depicted in Fig. 4. The algorithm and the coupling process could be performed even if we were to choose a different or even multiple reference points

on the structure. An impulse excitation was applied using a modal hammer with a hard metal tip (Fig. 7a), while the response was measured with a uni-axial accelerometer (Fig. 7b). During the measurement, six excitations were performed at each measuring point. Here it should be noted that no prede-

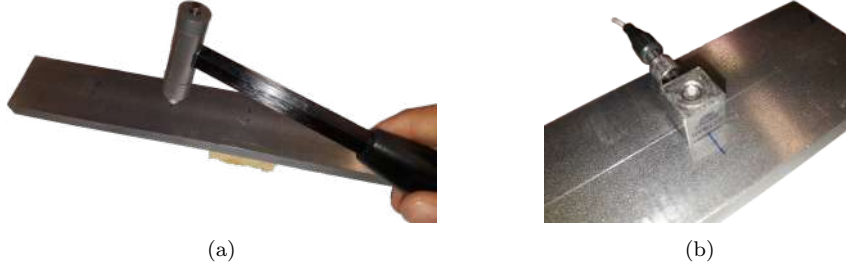


Figure 7: Photograph of the measurement equipment; a) Modal hammer PCB 086C03, b) Uni-axial accelerometer Dytran 3097A2T.

defined or intentional errors were introduced into the experimental response model.

The experimental model consisted of one row of the receptance matrix. For the measurement consistency identification algorithm, it would be sufficient to obtain an identically shaped receptance matrix of the numerical model. However, since the efficiency of the process is demonstrated by the final coupling of the two beams A with the LM FBS method, a square receptance matrix, including rotational DoFs, has to be included in the numerical model.

4.1. Identification of inconsistent measurements

To identify the inconsistent measurements, the proposed expansion method was applied at the locations of the measured points. One row, including only translational responses, was extracted from the full numerical model to establish the parent model (Fig. 6).

In the first part of the inconsistent-measurement identification algorithm, the iterative process is applied to reconstruct the removed FRFs based on the SEMM-expansion process. Next, the average coherence between the reconstructed measurements and the experimental counterparts is calculated. The coherence diagram of the analysed beam is shown in Fig. 8, where the boundary-coherence value was chosen to be 0.90. It should be emphasized that the value of the limit coherence criterion is case-specific and should be carefully selected with respect to the average coherence results. In the

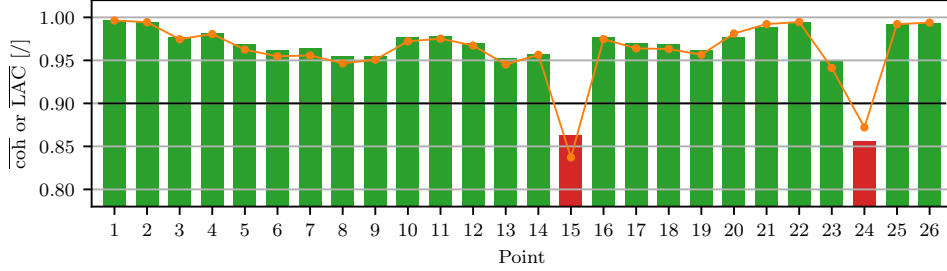


Figure 8: Average value of the coherence and LAC criterion.
 (■) - Consistent Measurement Coherence, (■) - Inconsistent Measurement Coherence,
 (—) - Boundary Coherence, (—○) - LAC

presented case, the identification algorithm was used to provide a consistent experimental model for the coupling process, which is very sensitive to experimental errors. For this reason, a high boundary coherence must be chosen, so that only the highest-quality measurements will be identified as consistent. In addition to the coherence criterion, the average value of the LAC criterion is also presented. It can be observed that the average LAC criterion results in similar correlation values between the reconstructed measurements and their experimental counterparts. By adopting the suggested limit, the measurements at points 15 and 24 are identified as inconsistent and should be removed from the existing experimental data set.

In order to confirm the selected boundary-coherence value, a statistical analysis using the box-plot method [28] was applied to the frequency-dependent coherence values. A box plot is a method of displaying statistical characteristics with quarters, where no statistical distribution is assumed. The basic element of the box plot is the median that delimits the lower from the upper half of the values in the data set. In our case a particular data set represents the coherence values at individual frequencies for a specific measuring point. The first quarter halves the lower half of the data set. It divides the complete data set so that 25% of the values are smaller and 75% larger. The third quarter delimits the upper half of the data set and thus represents a value, for which 75% are smaller and 25% larger.

Fig. 9 shows the interquartile range, a measure of the probability distribution. It stretches between the first and third quarters and represents an area where 50% of all the values are located. The line inside the box represents the median or second quarter. A large span of the interquartile range indicates significant changes in the coherence values within the observed frequency range for a given measurement.

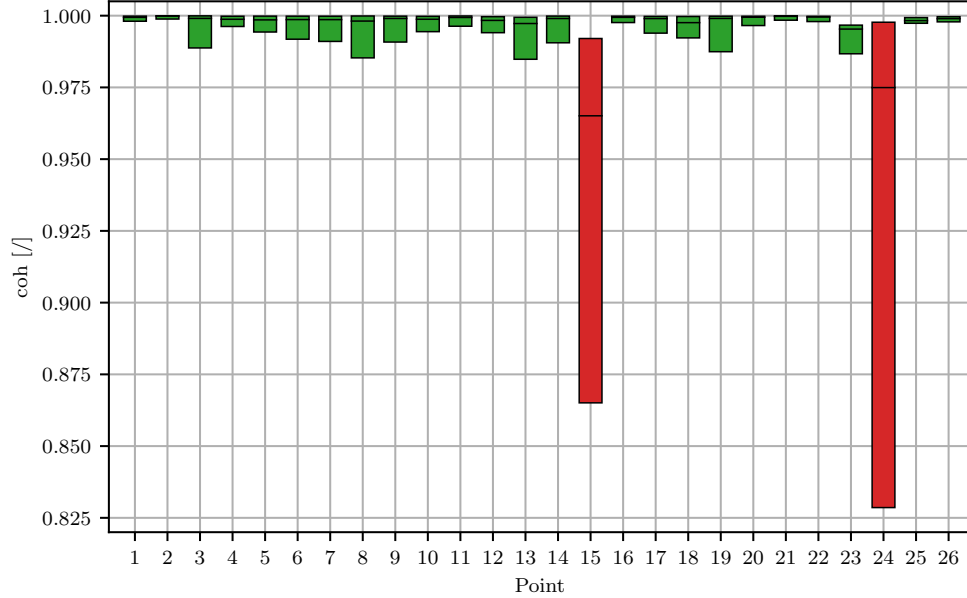
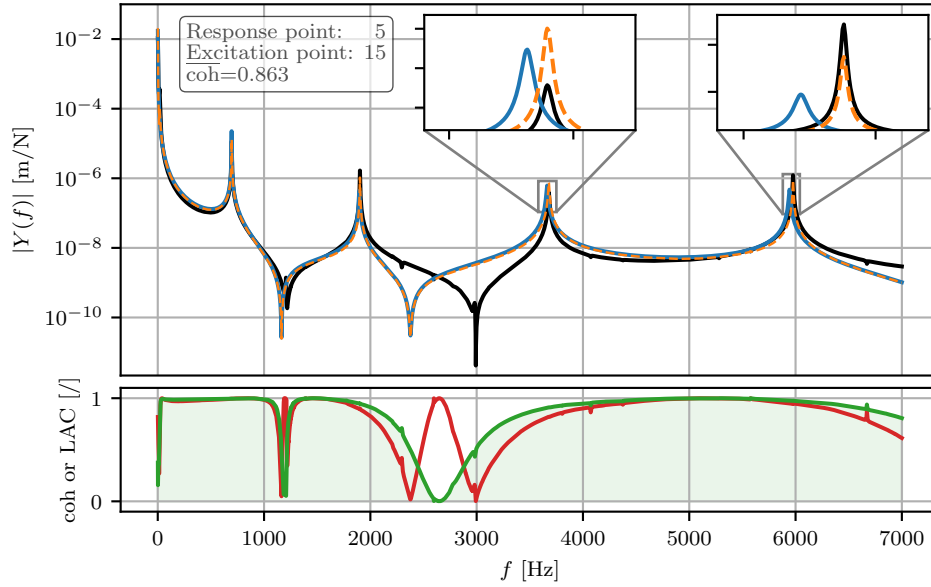
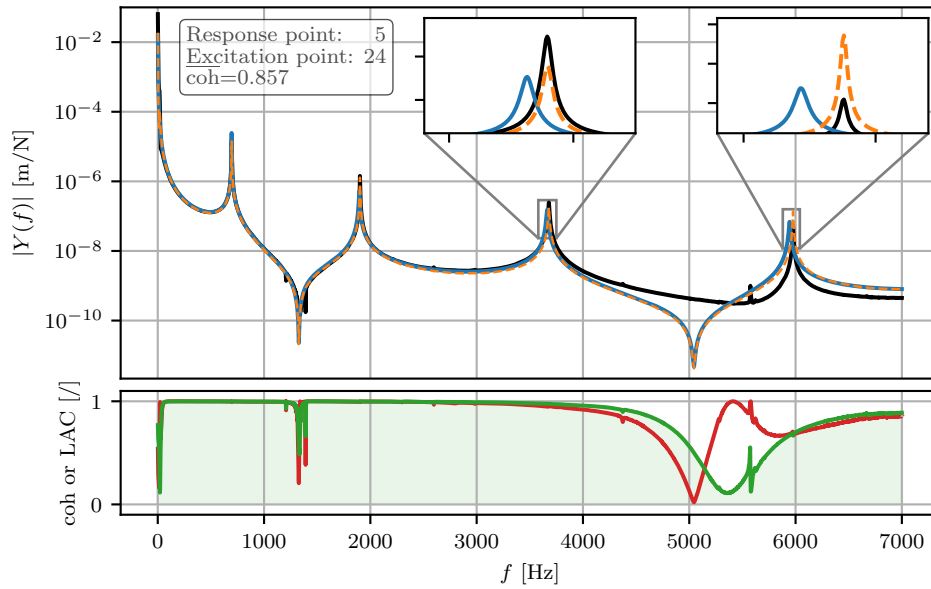


Figure 9: Representation of the coherence criterion in box-plot form, including only the interquartile range.
 (■) - Consistent Measurement, (■) - Inconsistent Measurement

It is evident (Fig. 9) that the interquartile ranges for points 15 and 24 are significantly larger than all the other points. By closely inspecting the FRFs and the coherence values of the reconstructed measurement and its experimental counterpart (Fig. 10), it becomes clear that the main difference is in the position of the anti-resonance regions. It can also be observed that the analysed FRFs correlate well in the resonance regions. The incorrect prediction of the measured FRFs in the anti-resonance regions is particularly problematic during the coupling process due to the inversion of the FRFs in the formulation. As shown in the continuation of the paper, this kind of inconsistent measurement can lead to an incorrect prediction of the final coupling results and should be omitted from the measurement set. Since the problem in both measurements lies in the misalignment of the anti-resonance regions, it is possible to relate the measurement error to a small misalignment of the impact or measuring location [2]. However, it should be noted that the aim of this paper is not to identify the nature of the measurement error, but to identify the inconsistent measurements in the experimental response model.



(a)



(b)

Figure 10: FRFs of inconsistent measurements and their reconstructed counterparts;

a) point 15, b) point 24.

(—) - Measurement, (—) - Numerical model, (---) - SEMM reconstruction
 (—) - coh, (—) - LAC

To demonstrate the difference between the consistent and inconsistent measurements, the comparison of the reconstructed measurement and its experimental counterpart is also presented for point 12 (Fig. 11). At this point, a high average coherence value and a low span of the interquartile range are observed, which indicates that the measurement is consistent. By closely inspecting the FRFs, it is obvious that the reconstructed measurement and its experimental counterpart correlate well in the resonance and the anti-resonance regions. Based on these observations it is evident that the box-plot method gives additional information about the average value of the coherence criterion, which represents a powerful tool to identify an inconsistent measurement in the experimental response model.

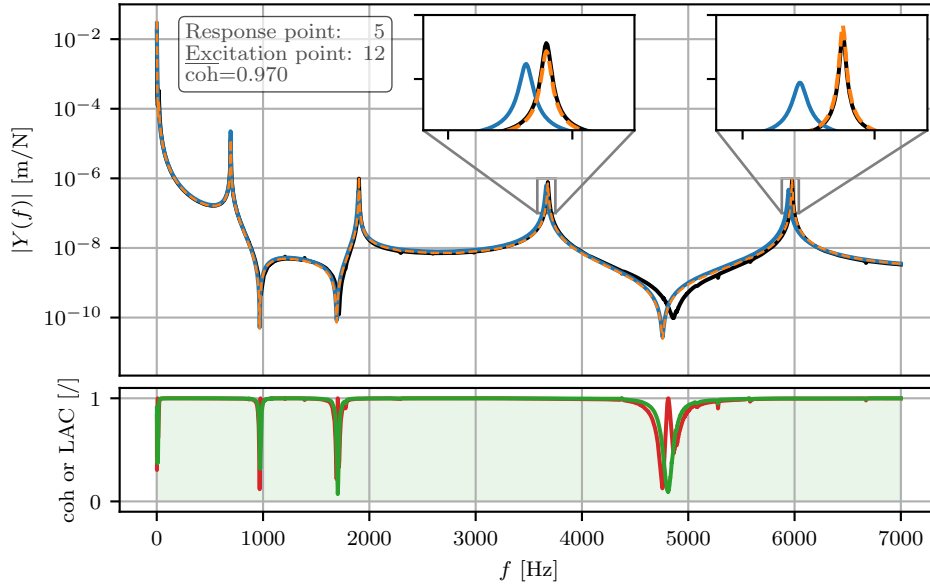


Figure 11: FRF of consistent measurement and its reconstructed counterpart at point 12.
 (—) - Measurement, (—) - Numerical model, (---) - SEMM reconstruction
 (—) - coh, (—) - LAC

Based on the presented example, the advantage of the proposed formulation for the identification of inconsistent measurements in the frequency domain becomes more evident. Since the measured FRFs are well aligned with the reconstructed counterparts in the region of the natural frequencies, this would require the use of advanced modal identification methods to identify misalignments in the FRFs between the natural frequencies. However, the presented algorithm makes it possible, by using only the frequency

domain, to evaluate the FRFs in the entire frequency range, including the regions between the natural frequencies. As shown in this example, even small inaccuracies in the position of the anti-resonance can be detected, which makes it possible to identify the inconsistent measurements in the experimental response model. As shown in the next section, this is of great importance for a reliable substructuring process.

4.1.1. Rejection performance of the proposed algorithm

In the previous section, the algorithm’s performance was demonstrated using an ”accurate” numerical model and an experimental response model with no intentionally imposed inconsistent measurements. Here, the efficiency of the algorithm-rejection performance is analysed by identifying inconsistent measurements using a less-accurate numerical model. In addition, in the experimental response model, the intentionally inconsistent measurements were introduced by considering sensor misalignment, setting the wrong gain of the sensors and random errors due to the presence of noise.

To obtain a less-accurate numerical model, the material parameters were slightly modified (Table 2) and unrealistic damping values were introduced by setting the Rayleigh proportional damping coefficient β to a high value. The comparison of experimental, numerical and reconstructed FRFs

Parameter	Value
L	300 mm
h	40 mm
t	12 mm
E	215 GPa
ρ	7800 kg/m ³
β	10 ⁻⁶ [/]

Table 2: Modified parameters of less-precise numerical model of beam A.

is shown in Fig. 12. The numerically obtained FRF is misaligned in terms of position and amplitude in the resonance regions. In the region of the third and fourth natural frequencies, this shift is higher than 100 Hz. Despite the introduction of the erroneous numerical model, the reconstructed FRF using the SEMM-expansion method agrees well with the experimentally obtained FRF. In the resonance regions, in particular, the positions of the peaks and the amplitudes are well aligned with the experimentally obtained FRF.

To demonstrate the robustness of the proposed algorithm, the same experimental response model presented in Section 4.1 was used in conjunction

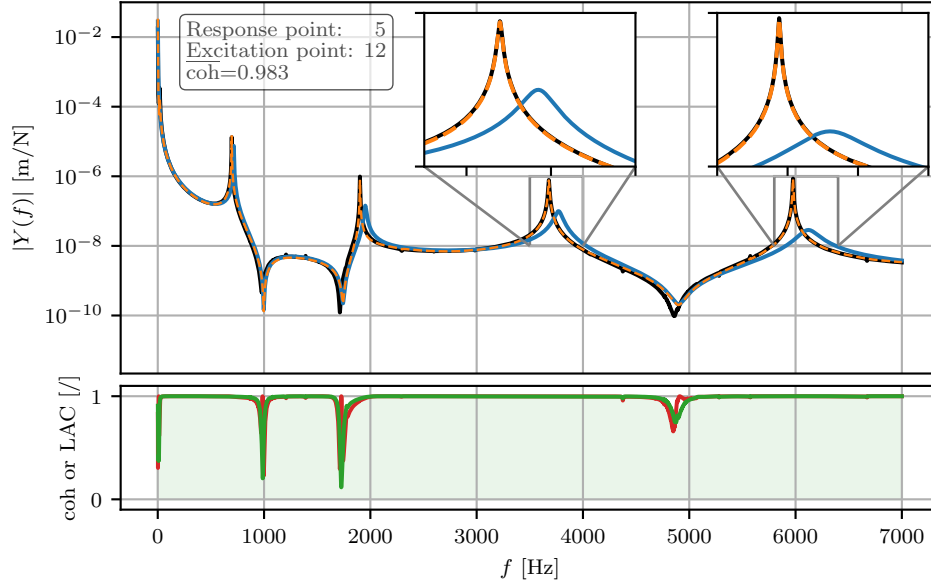


Figure 12: FRF comparison of measurement at point 12 and its reconstructed counterpart with FRF from a numerical model of poorer quality.
 (—) - Measurement, (—) - Numerical model, (---) - SEMM reconstruction
 (—) - coh, (—) - LAC

with a less-accurate numerical model. From the obtained coherence diagram in Fig. 13 it is evident that even with a less-accurate numerical model, the same measurements can be identified as inconsistent. Nevertheless, by com-

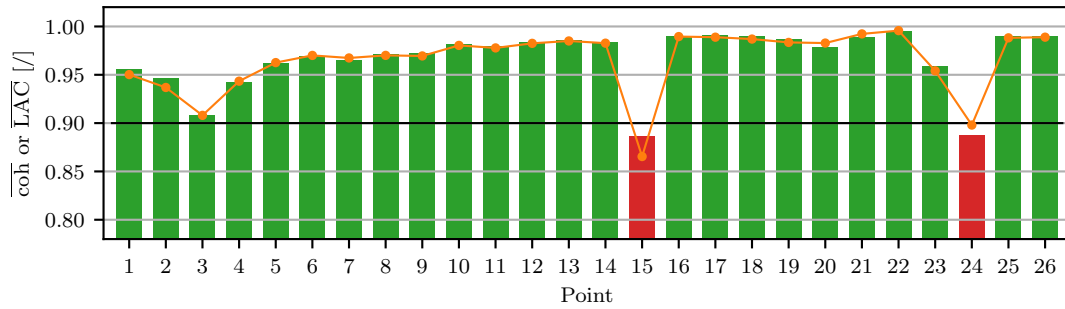


Figure 13: Coherence diagram in case of poorer numerical model.
 (■) - Consistent Measurement Coherence, (■) - Inconsistent Measurement Coherence,
 (—) - Boundary Coherence, (—○) - LAC

paring the coherence values (Fig. 8 and Fig. 13), it is clear that the use of the less-precise numerical model influences the accuracy of the SEMM-expansion process. For example, by inspecting the coherence values in point 3 (Fig. 13), it becomes apparent that the value is coming closer to the rejection limit and could potentially be identified as an inconsistent measurement. In these cases, it is recommended that this possible inconsistent measurement should be deleted rather than left in the experimental response model.

Additionally, the efficiency of the rejection process was examined by intentionally introducing the errors into the experimental response model. All the anomalies introduced at a given measurement point are detailed in Table 3. The proposed algorithm for identifying inconsistent measurements was performed using a less-accurate numerical model (Table 2).

Point	Error
4	erroneous sensor sign
8	swapped measurement from point 9 (wrong sensor wiring)
9	swapped measurement from point 8 (wrong sensor wiring)
11	erroneous sensor gain
19	excessive random errors (noise) in the measured signal

Table 3: Locations and types of errors intentionally introduced into the experimental model.

The obtained coherence diagram is shown in Fig. 14 and the comparison between the measured numerical results and the reconstructed FRF for all points with an imposed error are presented in Fig. 15. It is clear that all

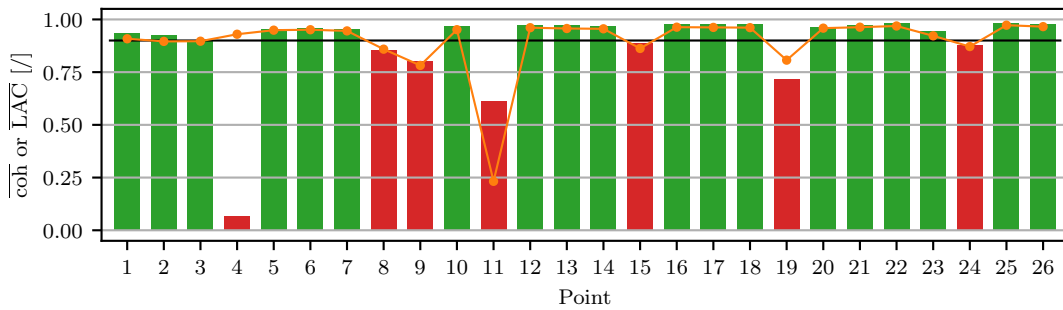


Figure 14: Identification of inconsistent measurement due to all possible errors.
 (■) - Consistent Measurement Coherence, (■) - Inconsistent Measurement Coherence,
 (—) - Boundary Coherence, (—○—) - LAC

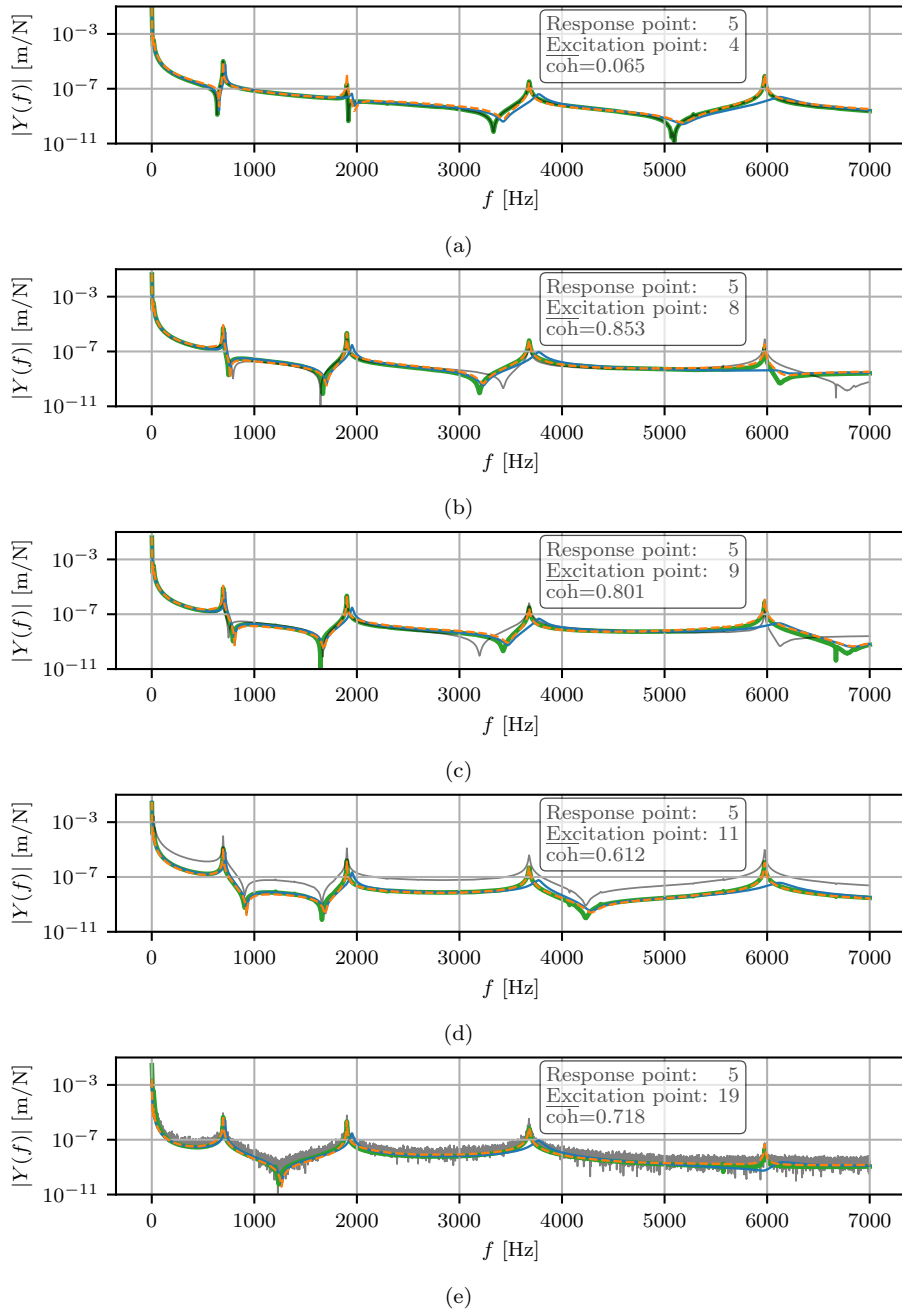


Figure 15: FRFs contaminated with different types of errors; a) erroneous sensor sign, b) swapped measurement from point 9, c) swapped measurement from point 8, d) erroneous sensor gain, e) excessive random errors.
 (—) - Erroneous measurement, (—) - Correct measurement, (—) - Numerical model, (---) - SEMM reconstruction

the measured points with intentionally introduced errors have significantly lower coherence values. By observing the coherence and LAC criteria at the same time, the inconsistent DoFs can be seen even more clearly. The measurement at point 4 contained an error of the wrong sign, which is not visible in the amplitude spectrum (Fig. 15a); therefore, this error cannot be detected with the LAC criterion as it is not phase sensitive. However, using the coherence criterion it is possible to identify this anomaly and to mark the measurement as inconsistent. By considering the measurement at point 11 where the faulty sensor gain was imposed (Fig. 15d), the LAC criteria, which correlate directly with the FRF amplitude, turn out to be more sensitive. However, even when using the coherence criterion it was possible to identify this type of error.

The measured FRFs at points 8 and 9, shown in Fig. 15b and 15c, are only 12 mm apart and were intentionally swapped (wrong sensor wiring). The proposed algorithm was able to detect this type of wrong sensor wiring at both the swapped locations. Finally, the noisy measurement (contaminated with random error) at point 19 (Fig. 15e) could also be detected with both criteria. From the LAC and coherence criterion this measurement can be clearly identified as inconsistent.

Finally, we can conclude that the proposed algorithm proves to be efficient even when the numerical model is not of high accuracy. In addition, it has been shown that the proposed algorithm can successfully detect different types of measurement errors.

4.2. *Dynamic coupling*

To show the efficiency of the proposed method for the identification of inconsistent measurements, two identical beams A were coupled using the LM FBS method to form a dynamic model of the coupled beam A-A (Fig. 17). The entire substructuring process is schematically presented in Fig. 16. The models used as input data are taken from Section 4.1. For the numerical model, a higher-quality form was used, while the experimental model was represented by measurements without intentionally added errors. First, the proposed algorithm for the identification of inconsistent measurements was applied to the system. Based on this algorithm, the measurements at points 15 and 24 were recognized as inconsistent (Fig. 8). Afterwards, two separate coupling processes were performed. The first coupling process included only consistent measurements, which excluded the measurements at points 15 and 24. The second coupling process included all the measurements in the experimental response model. In both cases, a full receptance matrix of

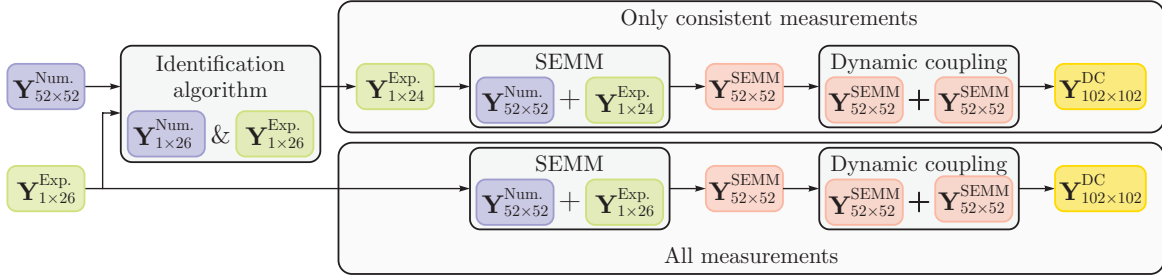


Figure 16: Schematic presentation of the coupling formulation.

beam A had to be obtained. The presence of rotational DoFs requires a rotation measurement and torque excitation, which proves to be a problematic process [29], thus some methods for an estimation of the rotational FRFs were developed [30]. For both coupling procedures, the SEMM-expansion process was performed based on the selected measurement set and the full numerical model.

Two identical beams A were coupled using the LM FBS method (Eq. (7)) proposing a rigid connection at the interface (Fig. 17). Hence, translation in the y -direction and the rotation about the z -axis were coupled at the interface of both beams A. To validate the coupling results, the reference experimental dynamic model of the coupled beam A-A was obtained independently. The excitation was performed at all 51 points in the y -direction, while the response was measured at point 5 (Fig. 17).

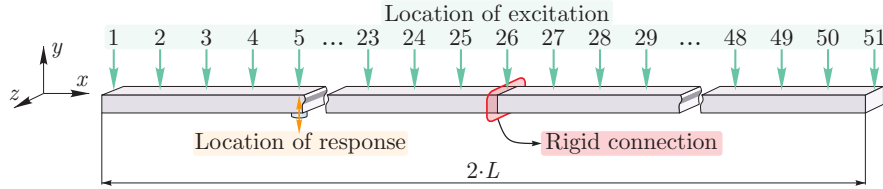
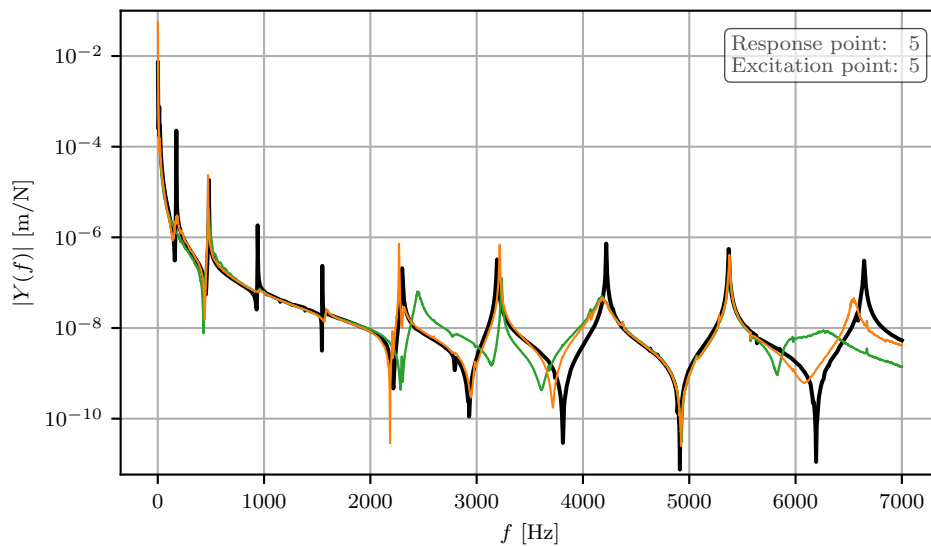
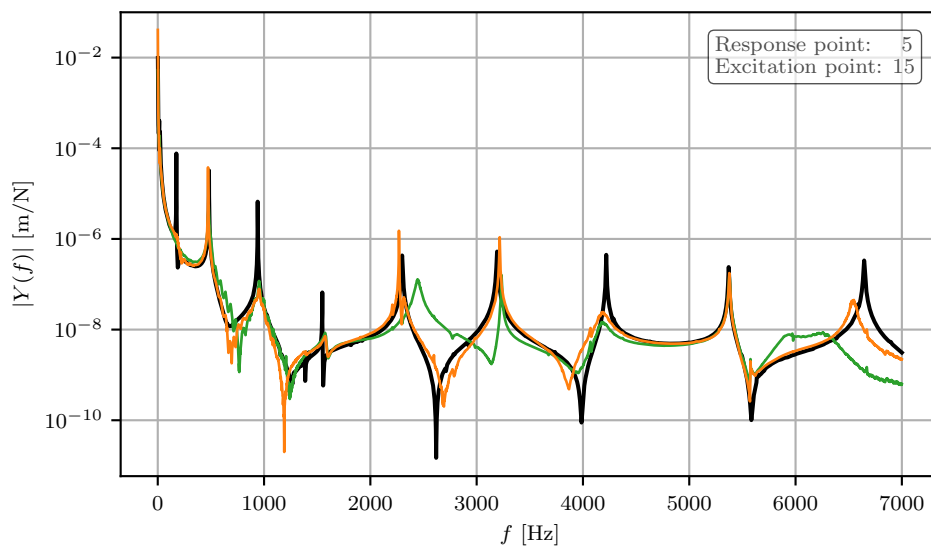


Figure 17: Schematic representation of the coupling process of beams A to the obtained coupled beam A-A.

An example of the coupled structure's dynamic response is shown in Fig. 18. The reference measurement was obtained by actually measuring the FRFs on the beam A-A. If all the measurements are considered in the coupling process, including the inconsistent ones, significant deviations from the reference measurements can be observed. The misalignment in terms of the amplitude and the position of the natural frequencies can be identified. Some natural frequencies cannot even be observed in the coupled dynamics



(a)



(b)

Figure 18: FRFs of coupled system; a) point 5, b) point 15.
 (—) - Reference Meas., (—) - SEMM - consistent Meas. (—) - SEMM - all Meas.

response (e.g., the natural frequency at 6800 Hz). The effect of measurement inconsistency on beam A at point 15 in the frequency range between 2000 and 4000 Hz and above 5000 Hz (Fig. 10a) is reflected in the FRFs of the coupled system. In these regions, the greatest deviations from the reference measurement can be observed.

If only consistent measurements are considered in the coupling process a fairly good matching with the reference FRFs can be identified. Particularly in the region between 2000 and 4000 Hz and above 5000 Hz, a better prediction of the coupled systems' dynamics response can be observed. All the natural frequencies can be identified and the position of the anti-resonance regions and their shape agree well with the reference measurement. An erroneous coupling result can be observed in the range of the first natural frequency (between 150 and 200 Hz) of the coupled system. The cause of the error stems from the characteristics of the experimental model, which is usually slightly less accurate in the lower frequency range, due to the dynamic properties of the experiment setup and the measuring range of the measuring equipment used. The solution to this problem is already included in the SEMM method, by introducing a trust function [5]. It makes it possible to shift the dynamic source to either the parent or overlay model. At low frequencies the provider of the dynamic properties is the numerical model, while the experimental model contributes the dynamic properties at higher frequencies. In this way, a more precise coupling is achieved even at lower frequencies.

To compare the overall agreement between the reference measurements and both coupling processes, an average coherence criterion versus the frequency is plotted (Fig. 19). The average criterion is obtained by computing the average value of all the measuring points at a given frequency. For the general case, it is calculated as:

$$\overline{\text{coh}}(f_k) = \frac{1}{p r} \sum_{i=1}^p \sum_{j=1}^r \text{coh}_{ij}(f_k), \quad (21)$$

where p represents the number of all the rows and r the number of columns of the response matrix of the coupled system. In our case, only the translational response at one point ($i = 5$) was considered experimentally ($p = 1$), which was deduced from the force excitation at all ($r = 51$) the points of the coupled system. Based on this representation of the coherence criterion, it can be observed that the value of the coherence criterion is higher for the entire frequency range. In particular, significantly higher coherence values can be observed in the range between 2000 and 4000 Hz and above 5000 Hz

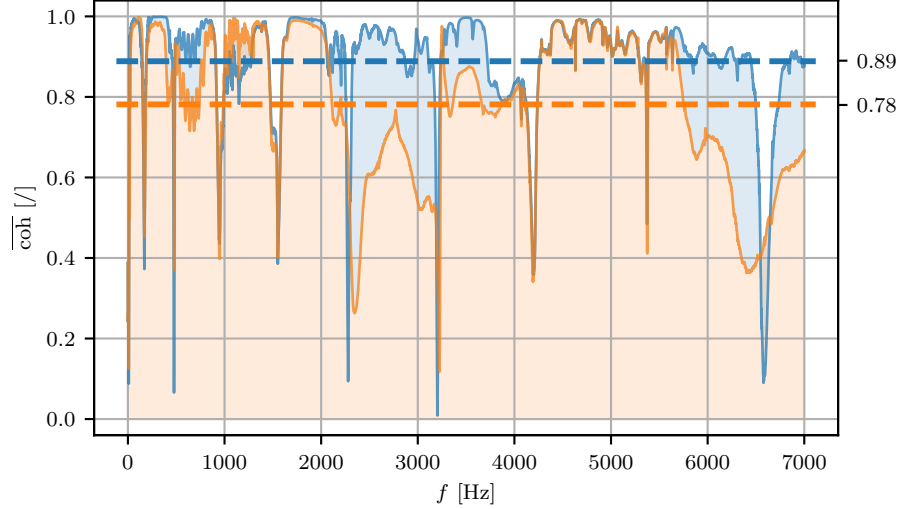


Figure 19: Average coherence criterion for all the measuring points versus frequency.

if the coupling is performed without inconsistent measurements. Based on the representation of the overall coherence value given by the equation:

$$\overline{\text{coh}} = \frac{1}{N} \sum_{k=1}^N \overline{\text{coh}}(f_k) \quad (22)$$

it is evident that if all the measurements are included in the coupling process the value is equal to 0.78. However, if the inconsistent measurements are excluded, the average coherence value increases to 0.89.

This experimental example shows that even a small number of inconsistent measurements can strongly influence the accuracy of the coupling process. Therefore, inconsistent measurements should be identified and omitted from the experimental response models. Finally, it is better to eliminate a potentially good measurement than to leave an inconsistent measurement in the experimental response model.

5. Conclusion

This work provides a framework for the identification of inconsistent measurements in the general experimental response model. Here, the application of the method on the frequency-based substructuring process is demonstrated. The algorithm identifies the inconsistent measurement based

on its comparison with the entire experimental response model. The method relies on removing the measurement from the experimental model and reconstructing it based on the remaining measurement set using the SEMM-expansion process. The developed equivalent numerical model of the system served only as part of the SEMM-expansion process and is not used for direct comparisons with the experimental model. Based on the correlation criterion between the reconstructed and the original measurement it was possible to identify an inconsistent measurement.

According to the presented experimental case study, it is evident that the identification of an inconsistent measurement is of great importance for an efficient and accurate substructuring process. It is shown that the measured sub-component FRF should be consistent across the entire frequency range and not just in the region of the natural frequencies. Since FRFs are used in the coupling process, even small inconsistencies can lead to an incorrect prediction of the coupled system's dynamics response.

Finally, it should be noted that the limit value of the correlation criterion should be selected conservatively, especially if the algorithm is used in the context of dynamic coupling. A high match limit will thus identify all the inconsistent measurements with greater certainty, which might include some good measurements. The absence of one potentially good measurement in the experimental model has very little effect on the coupling accuracy, while the presence of only one inconsistent measurement greatly reduces the coupling accuracy.

Acknowledgements

The authors acknowledge the partial financial support from the core research funding P2-0263 and applied research project L2-1837, both financed by ARRS, Slovenian research agency.

References

- [1] D. de Klerk, D. J. Rixen, S. Voormeeren, General framework for dynamic substructuring: history, review and classification of techniques, *AIAA journal* 46 (5) (2008) 1169–1181.
- [2] M. V. van der Seijs, Experimental dynamic substructuring: Analysis and design strategies for vehicle development, Ph.D. thesis, Delft University of Technology (2016).

- [3] J. W. R. Meggitt, On the treatment of uncertainty in experimentally measured frequency response functions, *Metrologia* 55 (6) (2018) 806–818.
- [4] D. de Klerk, D. J. Rixen, J. de Jong, The frequency based substructuring (FBS) method reformulated according to the dual domain decomposition method, in: *Proceedings of the 24th International Modal Analysis Conference, A Conference on Structural Dynamics*, 2006, pp. 1–14.
- [5] S. W. Klaassen, M. V. van der Seijs, D. de Klerk, System equivalent model mixing, *Mechanical Systems and Signal Processing* 105 (2018) 90–112.
- [6] M. S. Allen, D. Rixen, M. V. van der Seijs, P. Tiso, T. Abrahamsson, R. L. Mayes, *Substructuring in Engineering Dynamics*, Springer, 2020.
- [7] D. Nicgorski, P. Avitabile, Experimental issues related to frequency response function measurements for frequency-based substructuring, *Mechanical Systems and Signal Processing* 24 (5) (2010) 1324–1337.
- [8] T. Lim, J. Li, A theoretical and computational study of the FRF-based substructuring technique applying enhanced least square and TSVD approaches, *Journal of Sound and Vibration* 231 (4) (2000) 1135–1157.
- [9] T. G. Carne, C. R. Dohrmann, Improving experimental frequency response function matrices for admittance modeling, in: *Proceedings of the Nineteenth International Modal Analysis Conference*, 2006, pp. 143–156.
- [10] D. Nicgorski, P. Avitabile, Conditioning of FRF measurements for use with frequency based substructuring, *Mechanical Systems and Signal Processing* 24 (2) (2010) 340–351.
- [11] G. Čepon, A. Drozg, M. Boltežar, Introduction of line contact in frequency-based substructuring process using measured rotational degrees of freedom, in: *Journal of Physics: Conference Series*, Vol. 1264, IOP Publishing, 2019, p. 012025.
- [12] D. De Klerk, How bias errors affect experimental dynamic substructuring, in: T. Proulx (Ed.), *Structural Dynamics, Volume 3*, Springer New York, New York, NY, 2011, pp. 1101–1112.

- [13] P. Avitabile, *Modal testing: a practitioner's guide*, John Wiley & Sons, 2017.
- [14] S. Voormeeren, *Coupling procedure improvement & uncertainty quantification in experimental dynamic substructuring*, Master's thesis, TU Delft (2007).
- [15] D. De Klerk, *Dynamic response characterization of complex systems through operational identification and dynamic substructuring-an application to gear noise propagation in the automotive industry*, Ph.D. thesis, Delft University of Technology (2009).
- [16] J. M. M. e Silva, N. M. M. Maia, *Modal analysis and testing*, Vol. 363, Springer Science & Business Media, 2012.
- [17] W. Heylen, S. Lammens, *FRAC: a consistent way of comparing frequency response functions*, in: *International Conference on Identification in Engineering, 1996*, pp. 48–57.
- [18] R. J. Allemang, D. L. Brown, *A correlation coefficient for modal vector analysis*, in: *Proceedings of the 1st International Modal Analysis Conference, Vol. 1, 1982*, pp. 110–116.
- [19] N. Lieven, D. Ewins, *Spatial correlation of mode shapes, the coordinate modal assurance criterion (COMAC)*, in: *Proceedings of the 6th International Modal Analysis Conference, Vol. 1, Kissimmee Florida, USA, 1988*, pp. 690–695.
- [20] Y. Chen, P. Avitabile, J. Dodson, *Data consistency assessment function (DCAF)*, *Mechanical Systems and Signal Processing* 141 (2020) 106688.
- [21] S. Klaassen, M. V. van der Seijs, *Introducing SEMM: A novel method for hybrid modelling*, in: *Dynamics of Coupled Structures, Volume 4. Conference Proceedings of the Society for Experimental Mechanics Series*, Springer International Publishing, 2018, pp. 117–125.
- [22] S. W. B. Klaassen, D. J. Rixen, *The inclusion of a singular-value based filter in SEMM*, in: *Proceedings of the 38th International Modal Analysis Conference, A Conference on Structural Dynamics, 2020*.
- [23] H. Grafe, *Model updating of large structural dynamics models using measured response functions*, Ph.D. thesis, Imperial College of Science, Technology and Medicine, University of London (1999).

- [24] C. Zang, H. Grafe, M. Imregun, Frequency–domain criteria for correlating and updating dynamic finite element models, *Mechanical Systems and Signal Processing* 15 (1) (2001) 139–155.
- [25] C. Lein, M. Beitelschmidt, Comparative study of model correlation methods with application to model order reduction, in: *Proceedings 26th ISMA (International Conference on Noise and Vibration Engineering)*, 2014, pp. 2683–2700.
- [26] D. Lee, T.-S. Ahn, H.-S. Kim, A metric on the similarity between two frequency response functions, *Journal of Sound and Vibration* 436 (2018) 32–45.
- [27] M. V. van der Seijs, D. D. van den Bosch, D. J. Rixen, D. de Klerk, An improved methodology for the virtual point transformation of measured frequency response functions in dynamic substructuring, in: *4th ECCOMAS Thematic Conference on Computational Methods in Structural Dynamics and Earthquake Engineering (COMPADYN)*, 2013, pp. 4334–4347.
- [28] F. M. Dekking, C. Kraaikamp, H. P. Lopuhaä, L. E. Meester, *A Modern Introduction to Probability and Statistics: Understanding why and how*, Springer Science & Business Media, 2005.
- [29] A. Drozg, G. Čepon, M. Boltežar, Full-degrees-of-freedom frequency based substructuring, *Mechanical Systems and Signal Processing* 98 (2018) 570–579.
- [30] W. W. I. Mirza, M. A. Rani, M. Yunus, R. Febrina, M. Sani, Estimating rotational FRFs of a complex structure using FE model updating, mode expansion and FRF synthesis method, *IOP Conference Series: Materials Science and Engineering* 807 (2020) 012045.